GSA Data Repository 2019375; Bale, N.J., et al., 2019, Biomarker evidence for nitrogen-fixing cyanobacterial blooms in a brackish surface layer in the Nile River plume during sapropel deposition: Geology, v. 47, https://doi.org/10.1130/G46682.1

Supplement

METHODS

Collection of Suspended Particulate Matter (SPM)

McLane in situ pumps (McLane Laboratories Inc., Falmouth) were used to collect SPM from the water column for lipid analysis. They were deployed at 5 stations (Fig. 1) at 25 m depth with a cut-off at a pre-programmed pressure threshold and the SPM was collected on pre-ashed 0.3 µm or 0.7 µm (cf. Table S1) x 142 mm, GF/F filters (Pall Corporation, Port Washington, NY, USA) and immediately frozen at –80°C.

Bulk Sediment Elemental Composition of piston core 64PE406-E1

Sedimentary bulk elemental composition measurements were performed with an X-Ray Fluorescence (XRF) core scanning method for trace elements (Hennekam et al., 2019), calibrated to 40 inductively coupled plasma mass spectrometry measurements with the multivariate log-ratio calibration approach (Weltje et al., 2015). Elements are shown as concentrations and ratios to the terrestrial element Al to account for dilution effects by carbonate production.

Prior to analyses, the wet split core surfaces were flattened and covered with a thin SPEXCerti Ultralene foil. Subsequently, the XRF core scanning was performed in 1-cm resolution (10x10 mm slit size) using an Avaatech XRF core scanner equipped with state-of-the-art Rayspec cubed SiriusSD silicon drift detector with a 30 mm^2 collimated active area. The elements Ti and Al were measured at 20kV (Al filter), U was measured at 30kV (Pd-thick filter), and Ba and Mo were measured at 50kV (Cu filter), following (Hennekam et al., 2019). Daily measurements of 8 reference materials (GSR-4, GSR-6, GSD-10, JSd-1, JSd-3, MESS 3, SARM 2, and SARM 3), loosely pressed in polyethylene containers, indicated a relative standard deviation (i.e., precision) <10% for all elements.

The AvaaXelerate software (Bloemsma, 2015) was used to calibrate the XRF-core-scan data through multivariate log-ratio calibration (MLC). An automated calibration sample selection was run within the software, which resulted in a selection of 28 calibration sample depths that best represent the elemental variability within the whole core. Moreover, 12 extra sample depths were selected to ascertain more specifically a good representation of sapropel geochemistry. Subsequently, discrete samples from these 40 depth intervals (1-cm resolution) were dried, powdered, and totally digested in an $HClO_4$-HNO_3-HF acid mixture (following Reitz et al. (2006)). The digested samples in 1M HNO_3 were measured through inductively coupled plasma mass spectrometry (ICP-MS) with a Thermo Scientific Element 2 instrument. Standard samples (MESS-3 and JSd-3) showed an accuracy/precision (deviation from reference value; relative standard deviation) for the ICP-MS measurements: Al (<5%; ±1%), Ti (<7%; ±2%), Mo (<5%; ±2%), Ba (<6%;±1%), U (<4%; ±2%). Ultimately, the 40 samples measured through ICP-MS were used to calibrate the XRF-core-scan results with the MLC method.

The geochemical data are shown as concentrations and ratios, except for Ti/Al, which is only shown as a ratio. Normalization to Al is done to avoid closed-sum effects that may occur through variable fluxes in carbonate and organic components. These closed-sum effects are likely minor in the sapropel S5 interval in core 64PE406-E1, as indicated by the close resemblance of concentrations and ratios. Since Ti is not uniquely linked to sapropel deposition it is only shown as a ratio.

Age Model Construction of piston core 64PE406-E1

The age model of the S5 interval in the core is constructed using the well-defined age boundaries for the sapropels S4 (101.8-107.8 ka BP and its interruption at 104.0-105.4 ka BP) and S5 (121.5-128.3), following Grant et al. (2016) and Rodríguez-Sanz et al. (2017) for cores

LC21 and ODP967, respectively (See Figure S1a and b). Specifically, the deviations from the export-productivity proxy Barium and its ratio to Aluminum (Ba/Al), were used to tune these boundaries (Figure S1c), as these excursions were shown to be synchronous within age uncertainties (Rodríguez-Sanz et al., 2017). For the age interval prior to S5, we tuned the Ba/Al excursion in between sapropels S5 and S6 to that in Ziegler et al. (2010) (Figure S1d). As we focus on the sapropel S5 interval (320-400 cm in the core), here we only show the age interval from ~138.4 to ~117.8 ka BP.

Lipid Extraction and Analysis

The extraction of lipids from freeze dried sediment from the three cores and from SPM was carried out using a modified Bligh-Dyer extraction (Bale et al., 2018). HGs were analyzed by Ultra High Pressure Liquid Chromatography-High Resolution Mass Spectrometry (UHPLC-HRMS) using an Agilent 1290 Infinity I UHPLC equipped with thermostatted auto-injector and column oven, coupled to a Q Exactive Orbitrap MS with Ion Max source with heated electrospray ionization (HESI) probe (Thermo Fisher Scientific, Waltham, MA) (Bale et al., 2018). The Bligh-Dyer extracts from the three cores were re-dissolved before analysis in a mixture of heptane, isopropanol and water (72:27:1, v:v:v) which contained two internal standards (IS), a platelet-activating factor (PAF) standard (5 ng on column) and a short-chain glycolipid standard, n-dodecyl-β-D-glucopyranoside (≥98% Sigma-Aldrich, 20 ng on column; cf. Bale et al. (2017)). The samples were then filtered through 0.45 μm mesh True Regenerated Cellulose syringe filters (4 mm diameter; Grace Alltech). The injection volume was each sample was 10 μl. For quantification the relative response factor (RRF) between the n-dodecyl-β-D-glucopyranoside IS and an isolated C_6 HG (1-(O-hexose)-3,25-hexacosanediol (Bale et al., 2017) was determined to be 6.63.

Freeze dried sediments were decalcified in centrifuge tubes with 2M HCl for total organic carbon (TOC) analysis and analysis was carried out in tin cups using a Flash 2000 series elemental analyzer (Thermo Scientific) equipped with a Thermal Conductivity detector.

Diatom-Diazotroph Associations (DDAs) as a Source of C_6 HGs

Up to now, no C_6 HGs have been detected in the five cultures of diatom-diazotroph associations DDAs which have been analyzed for their HG (Schouten et al., 2013; Bale et al., 2015). However a supposed-symbiotic species of the heterocystous cyanobacteria *Calothrix* was isolated from the surface water of the tropical North Atlantic and was found to contain no detectable C_5 HGs but did contain C_6 HG_{28} triol and C_6 HG_{28} keto-diol and a novel HG_{28} triol with a methylated C_6 sugar (methyl HG_{28} triol; Bale et al. (2018)). None of these three HGs were detected in this study. Furthermore, the HG composition of the Atlantic *Calothrix* isolate is very similar to that described for a wide range of *Calothrix* cultures (Gambacorta et al., 1998; Bauersachs et al., 2009; Wörmer et al., 2012). Hence it is unlikely that the C_6 HG detected in the S5 sapropel are derived from either a *R. intracellularis* or *Calothrix* DDA.

Table S1. HG composition of core 64PE406-E1 and SPM from Eastern Mediterranean Sea (only HGs detected in this study shown in table). For comparison data from literature, i.e. Baltic Sea sediment and selected heterocystous cyanobacterial cultures. Key: ++ = dominant, + = present, tr. = trace, nd = not detected; nr = not reported. Av. = average.

Sample	C_5 HG_{30} triol	C_6 HG_{26} diol	C_6 HG_{28} diol	C_6 HG_{30} triol
64PE406-E1				
Av. after sapropel (n=5)	nd	nd	++	nd
Av. late sapropel (n=2)	++	nd	nd	nd
Av. mid sapropel (n=6)	++	tr.	++	+
Av. First half sapropel (n=10)	tr.	+	++	++
Av. before sapropel (n=7)	++	+	++	+
SPM E. Mediterranean				
Av. 25 m (n=5)	++	nd	nd	nd
Baltic Sea sediment[a]				
Modern warm period (MoWP)	nd	++	tr.	nr

Pre-MoWP brackish	nd	++	+	nr
Ancylus Lake	nd	++	nd /+/++	nr
Yoldia Sea	nd	++	+/++	nr
Cultures - DDAs				
Rhizosolenia clevei– Richelia intracellularis[b]	tr	nd	nd	nd
Hemiaulus hauckii–R. intracellularis[c]	++	nd	nd	nd
Hemiaulus membranaceous–R. intracellularis[c]	++	nd	nd	nd
Calothrix. sp. CCY1611 [d]	nd	nd	nd	nd
Cultures - Selected Nostocales (Free-living)				
Nodularia sp. CCY9414[e]	nr	++	nd	nd
Aphanizomenon aphanizomenoides UAM523[f]	nr	+	++	++
Aphanizomenon gracile UAM521[f]	nr	++	tr.	nd
Dolichospermum sp. CCY9402[e]	nr	nd	++	nd
Dolichospermum sp. 315 (formally *Anabaena*)[g]	nd	++	tr.	nd
Calothrix sp. MU27[f]	nr	nd	tr.	+
Calothrix sp. CCY9923[e]	nr	nd	+	nd

a= (Sollai et al., 2017), b = (Bale et al., 2015), c = (Schouten et al., 2013), d = (Bale et al., 2018), e = (Bauersachs et al., 2009), f = (Wörmer et al., 2012), g = (Bauersachs et al., 2017).

Table S2. Relative abundance of C_5 HG and C_6 HGs of total HGs in the S5 sapropel recovered in cores 64PE406-E1, MS66PC and ODP 160-971C-2H-3 (Fig. 1). The amount of *Hemiaulus hauckii* identified as percent of total diatoms (excl. *Chaetoceros* resting spores) is given for the ODP 160-971C-2H-3 (data from the supplementary information of Kemp et al. (1999)).

Core	Slice (depth in cm)	% C_5 HG	% C_6 HGs	% *Hemiaulus hauckii*
64PE406-E1	336-337	100	0	
	337-338	100	0	
	338-339	22	78	
	339-340	27	73	
	340-341	31	69	
	341-342	35	65	
	344-345	40	60	
	347-348	11	89	
	Av. upper part sapropel	**46 ± 35**	**54 ± 35**	**Not examined**
	349-350	4	96	
	352-353	4	96	
	355-356	2	98	
	357-358	2	98	
	359-360	1	99	
	362-363	3	97	
	365-366	4	96	
	367-368	2	98	
	368-369	8	92	
	369-370	5	95	
	Av. lower part sapropel	**3 ± 2**	**97 ± 2**	**Not examined**
MS66PC	123-124	12	88	
	126-127	12	88	
	128-129	15	85	
	132-133	12	88	
	Av. upper part sapropel	**13 ± 2**	**87 ± 2**	**Not examined**
	135-136	7	93	
	140-141	0	100	
	146-147	2	98	
	153-154	1	99	
	Av. lower part sapropel	**3 ± 3**	**97 ± 3**	**Not examined**
160-971C-2H-3	98-99	100	0	
	99-100	100	0	

	100-101	85	15	
	101-102	100	0	
	Av. upper part sapropel	**96 ± 7**	**4 ± 7**	**24 ± 3 (3 laminae)**
	125-126	35	65	
	126-127	26	74	
	127-128	14	86	
	128-129	13	87	
	Av. lower part sapropel	**22 ± 10**	**78 ± 10**	**1 ± 1 (17 laminae)**

C_5 HG = C_5 HG_{30} triol, C_6 HG = sum of C_6 HG_{26} diol, C_6 HG_{28} diol and C_6 HG_{30} triol. No attempt has been made to precisely align across the three cores the two periods (upper and lower half of sapropel). Av. = average.

REFERENCES

Bale, N.J., Hopmans, E.C., Dorhout, D., Stal, L.J., Grego, M., van Bleijswijk, J., Sinninghe Damsté, J.S., and Schouten, S., 2018, A novel heterocyst glycolipid detected in a pelagic N_2-fixing cyanobacterium of the genus Calothrix: Organic Geochemistry, v. 123, p. 44–47, doi:10.1016/j.orggeochem.2018.06.009.

Bale, N.J., Hopmans, E.C., Zell, C., Sobrinho, R.L., Kim, J.-H., Sinninghe Damsté, J.S., Villareal, T.A., and Schouten, S., 2015, Long chain glycolipids with pentose head groups as biomarkers for marine endosymbiotic heterocystous cyanobacteria: Organic Geochemistry, v. 81, p. 1–7, doi:10.1016/j.orggeochem.2015.01.004.

Bale, N., de Vries, S., Hopmans, E.C., Sinninghe Damsté, J.S., and Schouten, S., 2017, A method for quantifying heterocyst glycolipids in biomass and sediments: Organic Geochemistry, v. 110, p. 33–35, doi:10.1016/j.orggeochem.2017.04.010.

Bauersachs, T., Compaore, J., Hopmans, E.C., Stal, L.J., Schouten, S., and Sinninghe Damsté, J.S., 2009, Distribution of heterocyst glycolipids in cyanobacteria: Phytochemistry, v. 70, p. 2034–2039, doi:10.1016/j.phytochem.2009.08.014.

Bauersachs, T., Talbot, H.M., Sidgwick, F., Sivonen, K., and Schwark, L., 2017, Lipid biomarker signatures as tracers for harmful cyanobacterial blooms in the Baltic Sea: PLOS ONE, v. 12, p. e0186360, doi:10.1371/journal.pone.0186360.

Bloemsma, M.R., 2015, Development of a Modelling Framework for Core Data Integration using XRF Scanning: Delft Univeriesty of Technology, http://resolver.tudelft.nl/uuid:95a90787-edc7-4f1f-9e6a-b2453effabdb (accessed October 2018).

Gambacorta, A., Pagnotta, E., Romano, I., Sodano, G., and Trincone, A., 1998, Heterocyst glycolipids from nitrogen-fixing cyanobacteria other than Nostocaceae: Phytochemistry, v. 48, p. 801–805, doi:10.1016/S0031-9422(97)00954-0.

Grant, K.M., Grimm, R., Mikolajewicz, U., Marino, G., Ziegler, M., and Rohling, E.J., 2016, The timing of Mediterranean sapropel deposition relative to insolation, sea-level and African monsoon changes: Quaternary Science Reviews, v. 140, p. 125–141, doi:10.1016/j.quascirev.2016.03.026.

Hennekam, R., Sweere, T., Tjallingii, R., de Lange, G.J., and Reichart, G.-J., 2019, Trace metal analysis of sediment cores using a novel X-ray fluorescence core scanning method: Quaternary International, v. 514, p. 55–67, doi:10.1016/j.quaint.2018.10.018.

Kemp, A.E.S., Pearce, R.B., Koizumi, I., Pike, J., and Rance, S.J., 1999, The role of mat-forming diatoms in the formation of Mediterranean sapropels: Nature, v. 398, p. 57–61, doi:10.1038/18001.

Reitz, A., Thomson, J., Lange, G.J. de, and Hensen, C., 2006, Source and development of large manganese enrichments above eastern Mediterranean sapropel S1: Paleoceanography, v. 21, doi:10.1029/2005PA001169.

Rodríguez-Sanz, L., Bernasconi, S.M., Marino, G., Heslop, D., Müller, I.A., Fernandez, A., Grant, K.M., and Rohling, E.J., 2017, Penultimate deglacial warming across the

Mediterranean Sea revealed by clumped isotopes in foraminifera: Scientific Reports, v. 7, p. 16572, doi:10.1038/s41598-017-16528-6.

Schouten, S., Villareal, T.A., Hopmans, E.C., Mets, A., Swanson, K.M., and Sinninghe Damsté, J.S., 2013, Endosymbiotic heterocystous cyanobacteria synthesize different heterocyst glycolipids than free-living heterocystous cyanobacteria: Phytochemistry, v. 85, p. 115–121, doi:10.1016/j.phytochem.2012.09.002.

Sollai, M., Hopmans, E.C., Bale, N.J., Mets, A., Warden, L., Matthias Moros, and Sinninghe Damsté, J.S., 2017, The Holocene sedimentary record of cyanobacterial glycolipids in the Baltic Sea: an evaluation of their application as tracers of past nitrogen fixation: Biogeosciences, v. 14, p. 5789–5804, doi:https://doi.org/10.5194/bg-14-5789-2017.

Weltje, G.J., Bloemsma, M.R., Tjallingii, R., Heslop, D., Röhl, U., and Croudace, I.W., 2015, Prediction of Geochemical Composition from XRF Core Scanner Data: A New Multivariate Approach Including Automatic Selection of Calibration Samples and Quantification of Uncertainties, *in* Croudace, I.W. and Rothwell, R.G. eds., Micro-XRF Studies of Sediment Cores: Applications of a non-destructive tool for the environmental sciences, Dordrecht, Springer Netherlands, Developments in Paleoenvironmental Research, p. 507–534, doi:10.1007/978-94-017-9849-5_21.

Wörmer, L., Cires, S., Velazquez, D., Quesada, A., and Hinrichs, K.-U., 2012, Cyanobacterial heterocyst glycolipids in cultures and environmental samples: Diversity and biomarker potential: Limnology and Oceanography, v. 57, p. 1775–1788, doi:10.4319/lo.2012.57.06.1775.

Ziegler, M., Tuenter, E., and Lourens, L.J., 2010, The precession phase of the boreal summer monsoon as viewed from the eastern Mediterranean (ODP Site 968): Quaternary Science Reviews, v. 29, p. 1481–1490, doi:10.1016/j.quascirev.2010.03.011.

Figure S1. Records used for age model construction of the sapropel S5 interval in core 64PE406-E1: (a) LC21 $\delta^{18}O$ and Soreq cave $\delta^{18}O$ (Grant et al., 2016), (b) LC21 (41-point moving average) and ODP967 Ba counts from XRF-scanning (Rodriguez-Sanz et al., 2017), (c) 64PE406-E1 Ba concentration and ratio to Al (this study), (d) ODP968 Ba/Al (Ziegler et al., 2010), (e) Age (in ka) versus depth (cm) calculated using the age model based on our tie-points. The tie-points (red circles) used to link the Ba-derived excursions to those same excursions in 64PE406-E1 are indicated.

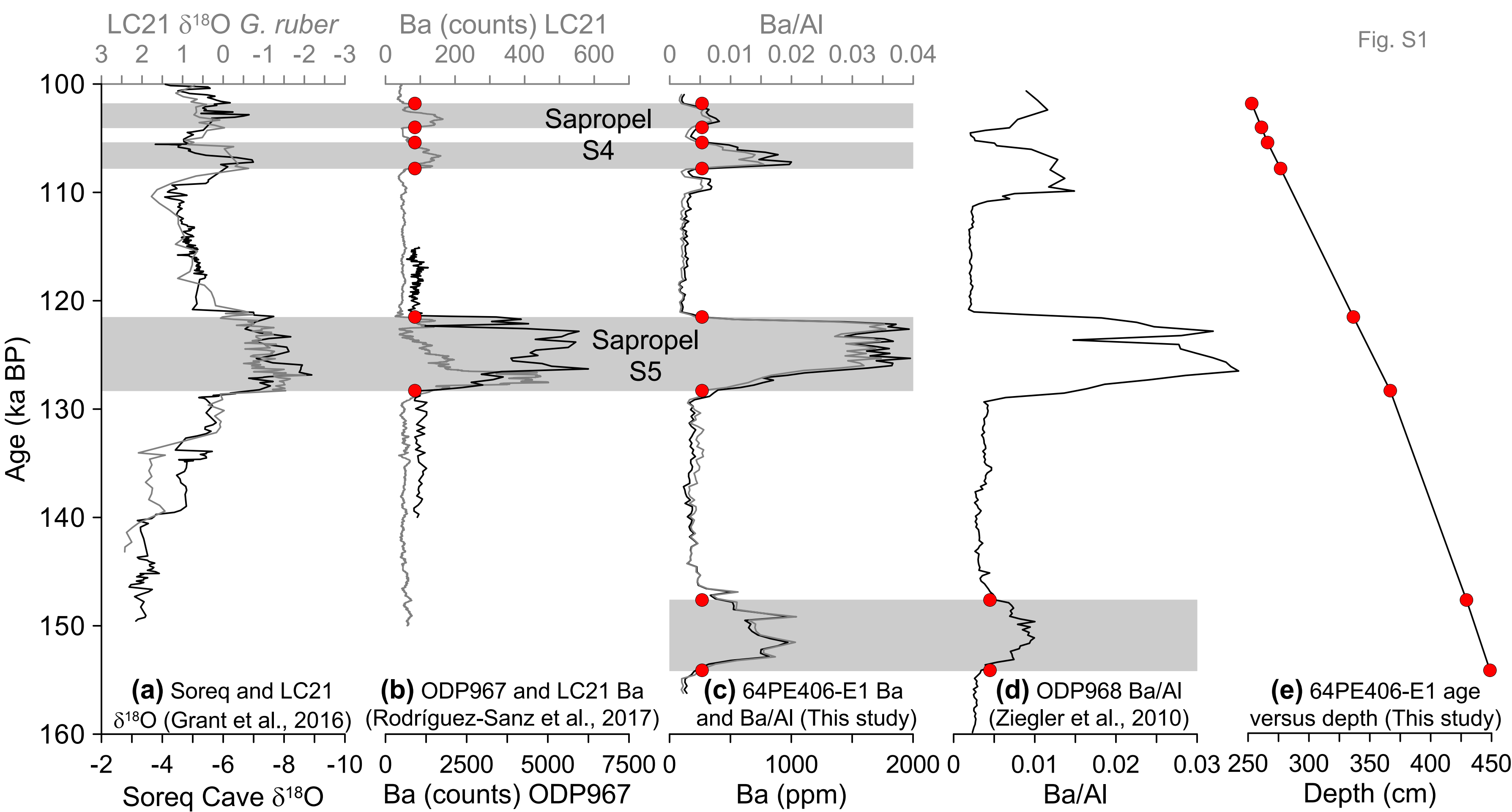
Fig. S1
LC21 δ18O G. ruber
3 2 1 0 -1 -2 -3
Ba (counts) LC21
0 200 400 600
Ba/Al
0 0.01 0.02 0.03 0.04
Sapropel S4
Sapropel S5
Age (ka BP)
100 110 120 130 140 150 160
(a) Soreq and LC21 δ18O (Grant et al., 2016)
(b) ODP967 and LC21 Ba (Rodríguez-Sanz et al., 2017)
(c) 64PE406-E1 Ba and Ba/Al (This study)
(d) ODP968 Ba/Al (Ziegler et al., 2010)
(e) 64PE406-E1 age versus depth (This study)
-2 -4 -6 -8 -10
Soreq Cave δ18O
0 2500 5000 7500
Ba (counts) ODP967
0 1000 2000
Ba (ppm)
0 0.01 0.02 0.03
Ba/Al
250 300 350 400 450
Depth (cm)